

Parametric Schemes for Prediction of Wideband MIMO Wireless Channels

Ramoni Adeogun, *Student Member, IEEE*, Paul Teal, *Senior Member, IEEE*
and Pawel Dmochowski, *Senior Member, IEEE*

Abstract—Information on the future state of time varying frequency selective channels can significantly enhance the effectiveness of feedback in adaptive and limited feedback MIMO-OFDM systems. This paper investigates the parametric extrapolation of wideband MIMO channels using variations of the double directional MIMO model. We propose three predictors which estimate parameters of the channel using 4D, 3D and 2D extensions of the ESPRIT algorithm and predict future states of the channel using the models. Furthermore, using the vector formulation of the Cramer Rao lower bound for functions of parameters, we derive a bound on the prediction error in wideband MIMO channels. Numerical simulations are used to evaluate the performance of the proposed algorithms under different channel and transmission conditions, and a comparison is made with the derived error bound.

Index Terms—Channel prediction, multidimensional parameter estimation, multipath fading, ESPRIT, frequency selective channel.

I. INTRODUCTION

THE combination of MIMO transmission with Orthogonal Frequency Division Multiplexing (OFDM) [1] is a spectrally efficient technique for achieving reliable high bit rate transmission over mobile wideband channels. It is employed in wireless standards such as 3GPP LTE and LTE Advanced [2], IEEE 802.16e (WiMAX) [3, 4]. Recent capacity approaching MIMO-OFDM based transmission schemes, such as adaptive MIMO precoding [5], adaptive coding and modulation, adaptive multiuser resource allocation and scheduling [6, 7] and various forms of codebook and non-codebook based limited feedback MIMO, require both at the transmitter and the receiver knowledge of the channel state information (CSI). In time division duplex (TDD) systems, channel reciprocity is used to obtain CSI. In frequency division duplex (FDD) systems however, CSI is estimated at the receiver and relayed in quantized form to the transmitter via a low rate feedback link. In practical MIMO systems, due to delays in estimation, processing and feedback, the CSI may become outdated before its actual use at the transmitter, resulting in significant performance degradation especially in high mobility environments. Prediction of the CSI has been recognised as an effective technique for mitigating this performance degradation [8, 9].

The problem of channel prediction for single input single output (SISO) channels has been studied extensively. In [8, 10, 11], the narrowband SISO channel is modelled as an autoregressive (AR) process and a linear minimum mean squared

error (MMSE) predictor is used to extrapolate the channel states. These schemes consider the time-varying channel as a stochastic wide sense stationary process and use the temporal correlation for prediction without accounting for the physical scattering phenomena that cause the fading. Other researchers [12–14] have considered a ray based sum of sinusoids model where the fading channel is modelled as a sum of a finite number of plane waves. Extensions of these algorithms to wideband SISO channels have also been studied [15, 16]. Analytical and simulation results on SISO prediction have proven that with dense scattering, SISO channels can only be predicted over a very short distance (on the order of tenths of a wavelength) depending on the environment and propagation scenarios. The bound on SISO channel prediction error [17] indicates that CSI is required over several wavelengths in order to accurately predict the channel. It has also been shown that prediction beyond a wavelength is not realistic, particularly in practical cases where the stationarity assumption does not hold for a time comparable to the duration of the observation.

The prediction of multi-antenna channels was first investigated in [18] through an evaluation of downlink beamforming with channel prediction. Improved MISO channel prediction was shown, as more structure of the wavefield is revealed through multiple sampling. Bounds on the prediction error of MIMO channels [19] and MIMO-OFDM channels [20] indicate that better prediction can be obtained by utilizing the channel spatial structure. The authors illustrated this using AR modelling for the prediction of beamspace transformed CSI, and argue that the transformation reduces the effective number of rays present in the channel, ultimately resulting in longer prediction. A similar approach based on ray cancelling was presented in [21].

MIMO prediction schemes can be broadly classified into codebook based precoder prediction and non-codebook based CSI prediction. The codebook based schemes [22, 23] predict the precoder for the next transmission frame using linear prediction. Others adopt Givens rotations to transform the precoding matrix and perform prediction of the Givens parameter [24]. These schemes are limited to one step prediction and the channel model is often assumed to be independent and identically distributed (i.i.d). Non-codebook based schemes predict the actual CSI using either autoregressive modelling or parametric model based SISO approaches [25]. These methods do not utilize the additional spatial information that is revealed by the presence of multiple sensors.

Motivated by the results in [20, 26], where it was shown using error bounds that schemes which incorporate both temporal

The authors are with the School of Engineering and Computer Science, Victoria University of Wellington, Wellington, New Zealand. e-mail: {ramon.adeogun, pawel.dmochowski, paul.teal}@ecs.vuw.ac.nz

and spatial channel information offer significant improvement in prediction performance, we make the following contributions in this paper.

- Using a double directional spatial channel model, we derive three formulations of prediction models by progressively removing the dependence on array geometry. This allows the investigation of the effects of transmit and/or receive spatial dimensions on prediction performance, and the development of schemes applicable to systems with different antenna geometries.
- We propose prediction schemes based on the above models and original adaptations of multidimensional ESPRIT (estimation of signal parameters via rotational invariance techniques) [27]. We show that this approach allows for the resolution of many more paths than the number of antennas at both ends of the link.
- Using the vector formulation of the Cramer Rao bound for functions of parameters, we derive an expression for the bound on the prediction error. Although similar analyses have been presented in [20, 26], our formulations are simpler and easier to interpret.

The remainder of the paper is organized as follows. Section II presents different formulations of the double directional channel model for wideband MIMO systems. In Section III, we describe the data transformation and preprocessing required for the implementation of the proposed schemes. The channel predictors are presented in Section IV, followed by a derivation of the bound on prediction error in Section V. Performance evaluation results and discussion are given in Section VI. Finally, we draw conclusions in Section VII.

II. CHANNEL MODELS

We consider several formulations of a ray-based wideband spatial MIMO channel model for the development of the prediction schemes in this paper. The formulations are extensions of the continuous time impulse response of doubly selective SISO fading channels, defined as

$$h(t; \tau) = \sum_{p=1}^P \alpha_p(t) \delta(\tau - \tau_p(t)) \quad (1)$$

where t and τ are the time and delay variables respectively, P is the number of paths, and $\alpha_p(t)$ and $\tau_p(t)$ are the time-varying complex attenuation and delay of the p th path, respectively. We assume that the scattering sources are in the far field of both the transmit and receive antenna arrays such that the propagating waves can be modelled as plane waves. The complex attenuation of the p th path can thus be defined as

$$\alpha_p(t) = \sum_{r=1}^{R_p} \beta_{r,p} \exp(j\nu_{r,p}t) \quad (2)$$

where R_p is the number of rays in the p th path, $j = \sqrt{-1}$, $\beta_{r,p}$ and $\nu_{r,p}$ are the complex amplitude and Doppler frequency of the r th ray in the p th path, respectively. The model in (2) can be extended to a MIMO channel with M transmit and N

receive antennas via the introduction of transmit and receive array structures, giving

$$\mathbf{H}_p(t) = \sum_{r=1}^{R_p} \beta_{r,p} \mathbf{a}_r(\theta_{r,p}) \mathbf{a}_t^T(\phi_{r,p}) \exp(j\nu_{r,p}t) \quad (3)$$

where $[\cdot]^T$ denotes the non-conjugate transpose of the associated matrix, $\mathbf{a}_r(\theta_{r,p})$ and $\mathbf{a}_t(\phi_{r,p})$ are the receive and transmit array response vectors and $\theta_{r,p}$ and $\phi_{r,p}$ are the directions of arrival and directions of departure, respectively. Summing (3) over the clusters and taking the Fourier transform in the delay domain, we obtain the frequency response of the MIMO channel as

$$\begin{aligned} \mathbf{H}(t, f) &= \sum_{p=1}^P \mathbf{H}_p(t) \exp(-j2\pi f \tau_p) \\ &= \sum_{p=1}^P \sum_{r=1}^{R_p} \beta_{r,p} \mathbf{a}_r(\theta_{r,p}) \mathbf{a}_t^T(\phi_{r,p}) \exp(j\nu_{r,p}t - j2\pi f \tau_p) \end{aligned} \quad (4)$$

where f is the frequency variable. Assuming symbol duration Δt and subcarrier spacing Δf , the sampled frequency response is given by

$$\mathbf{H}(q, k) = \sum_{p=1}^P \sum_{r=1}^{R_p} \beta_{r,p} \mathbf{a}_r(\theta_{r,p}) \mathbf{a}_t^T(\phi_{r,p}) \exp(jq\gamma_{r,p} - jk\eta_p) \quad (5)$$

where $q = 0, \dots, Q-1$ and $k = 0, \dots, K-1$ are the time and subcarrier indices, respectively. $\gamma_{r,p} = \nu_{r,p}\Delta t$ and $\eta_p = 2\pi\Delta f\tau_p$ are the normalized radian Doppler frequency and delay, respectively. Combining indices in (5), we obtain

$$\mathbf{H}(q, k) = \sum_{z=1}^Z \beta_z \mathbf{a}_r(\theta_z) \mathbf{a}_t^T(\phi_z) \exp(jq\gamma_z - jk\eta_z) \quad (6)$$

where $Z = \sum_{p=1}^P R_p$ is the total number of propagating rays. Each ray is characterized by the parameter set $\{\beta_z, \theta_z, \phi_z, \gamma_z, \eta_z\}$. We assume that no two rays share a common parameter set, but different rays may have one or more equal parameters. Note that in practical scenarios, (6) has a finite support in the transmit angular, Doppler, delay and receive angular domains since the multipath parameters are bounded.

We now describe different formulations of the model in (6), where we progressively remove restrictions on the array structure.

A. DOD/DOA Model

The first model is based on the assumption that the array response vectors \mathbf{a}_r and \mathbf{a}_t are explicit functions of the directions of arrival (DOA) and directions of departures (DOD) [26] as shown in (6). Note that this model is valid for any array geometry. We will consider systems with uniform linear arrays (ULA) at both ends of the link. The receive steering vector for an N element array is thus

$$\mathbf{a}_r(\mu_z^r) = [1, \exp(j\mu_z^r), \dots, \exp(j(N-1)\mu_z^r)]^T \quad (7)$$

where

$$\mu_z^r = 2\pi d_r \sin(\theta_z), \quad (8)$$

d_r is the receive array element spacing. The $M \times 1$ transmit array steering vector is defined analogously, with

$$\mu_z^t = 2\pi d_t \sin(\phi_z) \quad (9)$$

Here, d_t is the transmit array element spacing. Henceforth, the parameter set for the models will include the spatial frequencies μ_z^r and μ_z^t rather than the actual directions θ_z and ϕ_z , since the latter can be trivially obtained from μ_z^r, μ_z^t using (8) and (9).

B. Transmit Spatial Signature Model (TSSM)

The DOD/DOA model depends on the specific array configurations and the angles of arrival and departure. Since the transmitter is often stationary in mobile wireless systems, estimation of the angles of departure may be difficult and possibly not required for accurate prediction of the channel. We therefore replace the product of the complex amplitude and the transmit array steering vector for each path in (6) by an unstructured transmit spatial signature (TSS)¹ vector, \mathbf{s} . The model in (6) can now be expressed as

$$\mathbf{H}(q, k) = \sum_{z=1}^Z \mathbf{a}_r(\mu_z^r) \mathbf{s}_z^T \exp(jq\gamma_z - jk\eta_z) \quad (10)$$

where $\mathbf{s}_z \in \mathbb{C}^{M \times 1}$ is the TSS for the z th propagating wave.

C. Matrix Spatial Signature Model (MSSM)

Similar to the TSS model, the MSSM [26] replaces the product of the array steering vectors by an $N \times M$ unstructured matrix spatial signature, \mathbf{S} , giving

$$\mathbf{H}(q, k) = \sum_{z=1}^Z \mathbf{S}_z \exp(jq\gamma_z - jk\eta_z) \quad (11)$$

Note that although the three models described in this section are derived from the double directional MIMO model, they differ in the parametrization and number of parameters required. A summary of the number of parameters required for each model and dependence on number of antenna elements is shown in Table I. The parameters of the channel are assumed quasi-stationary over the spatial distance for which channel observation/measurement and prediction is made. This assumption has been shown in the industry standard 3GPP/WINNER II SCM model [28, p. 55] to be valid for mobile movements up to 50λ . We also assume that Q temporal samples and K frequency samples of the channel frequency response matrix are available by transmitting known training sequences or from other channel estimation approaches.

In practice, the estimated or measured channel will be imperfect due to the effects of noise and interference. The estimated CSI matrix at time instant q for the k th subcarrier is therefore defined as²

$$\hat{\mathbf{H}}(k, q) = \mathbf{H}(k, q) + \mathbf{N}(k, q) \quad (12)$$

¹A similar model termed vector spatial signature (VSS) was used in [26].

²Henceforth, we use $\hat{\cdot}$ to denote estimates corrupted by noise.

TABLE I: MIMO Model Parametrization and Dependence on Number of Antennas

Model	Structural Param.	Amp.	Real Param.
DOD/DOA	$\{\mu_z^r, \mu_z^t, \gamma_z, \eta_z\}_{z=1}^Z$	$\{\Re(\beta_z), \Im(\beta_z)\}_{z=1}^Z$	$6Z$
TSSM	$\{\mu_z^r, \gamma_z, \eta_z\}_{z=1}^Z$	$\{\Re(\mathbf{s}_z), \Im(\mathbf{s}_z)\}_{z=1}^Z$	$Z(2M + 3)$
MSSM	$\{\gamma_z, \eta_z\}_{z=1}^Z$	$\{\Re(\mathbf{S}_z), \Im(\mathbf{S}_z)\}_{z=1}^Z$	$2Z(NM + 1)$

where $\mathbf{N}(k, q) \in \mathbb{C}^{N \times M}$ is a matrix of complex Gaussian random variables that accounts for channel estimation errors.

III. DATA TRANSFORMATION

Having described the channel model variations for the development of the prediction schemes, we now present the data preprocessing necessary for extraction of the parameters from available channel observations.

A. DOD/DOA Transformation

As shown in (6), the DOD/DOA model is characterized by $4Z$ structural parameters $\{\mu_z^r, \mu_z^t, \gamma_z, \eta_z\}_{z=1}^Z$ and Z complex amplitudes. Extraction of these parameters from the channel observations requires a four dimensional array data structure. Since we consider MIMO systems with a 1-D antenna array (i.e., a ULA) at both ends of the link, it is necessary to convert the channel matrices into a form that allows 4D parameter estimation to be performed. Let $\mathbf{h}(q, k) = \text{vec}[\mathbf{H}(q, k)] \in \mathbb{C}^{NM \times 1}$ be a vector obtained by stacking the columns of $\mathbf{H}(q, k)$. Using (6) and the properties of the Kronecker product, it can be shown that

$$\mathbf{h}(q, k) = \sum_{z=1}^Z \beta_z (\mathbf{a}_r(\mu_z^r) \otimes \mathbf{a}_t(\mu_z^t)) \exp(jq\gamma_z - jk\eta_z) \quad (13)$$

where \otimes denotes the Kronecker product. Note that the transformation in (13) combines the receive and transmit spatial dimension of the channel. In order to introduce the temporal dimension, we define

$$\mathbf{D}(k) = [\mathbf{h}(1, k) \quad \mathbf{h}(2, k) \quad \cdots \quad \mathbf{h}(Q, k)] \quad (14)$$

and form a Hankel matrix by sliding an $NM \times R$ rectangular window through (14) to obtain

$$\mathbf{D}_k = \begin{bmatrix} \mathbf{h}(1, k) & \mathbf{h}(2, k) & \cdots & \mathbf{h}(R, k) \\ \mathbf{h}(2, k) & \mathbf{h}(3, k) & \cdots & \mathbf{h}(R+1, k) \\ \vdots & \vdots & \ddots & \vdots \\ \mathbf{h}(S, k) & \mathbf{h}(S+1, k) & \cdots & \mathbf{h}(Q, k) \end{bmatrix} \quad (15)$$

where $S = Q - R + 1$. The frequency dimension of the channel is similarly introduced by forming a block Hankel matrix from K such matrices to obtain

$$\mathbf{X}_d = \begin{bmatrix} \mathbf{D}_1 & \mathbf{D}_2 & \cdots & \mathbf{D}_T \\ \mathbf{D}_2 & \mathbf{D}_3 & \cdots & \mathbf{D}_{(T+1)} \\ \vdots & \vdots & \ddots & \vdots \\ \mathbf{D}_U & \mathbf{D}_{(U+1)} & \cdots & \mathbf{D}_K \end{bmatrix} \quad (16)$$

where U and T are the Hankel matrix size parameters with $U = K - T + 1$. The values of S, R, T , and U are selected such

TABLE II: Wideband MIMO Data Domain and Parameters

Model	Data Domain			
	Receive	Transmit	Temporal	Frequency
DOA/DOD	AOA	AOD	Doppler Shift	Delay
TSSM	AOA	-	Doppler shift	Delay
MSSM	-	-	Doppler shift	Delay

that $NMSU \geq Z + 1$. There is, however, a compromise in selecting these: large values of S and U increases the number of rows in \mathbf{X}_d and hence the number of sources that can be resolved, but this results in small values of R and T which affects the accuracy of covariance estimates. Using the model in (13) and the transformations in (15) and (16), the data in the columns of \mathbf{X}_d can be modelled as

$$\mathbf{x}_d(i) = \sum_{z=1}^Z \beta_z \mathbf{a}(\mu_z^r, \mu_z^t, \gamma_z, \eta_z) \exp(-j(i-1)\eta_z) \quad (17)$$

where $\mathbf{a}(\mu_z^r, \mu_z^t, \gamma_z, \eta_z) = (\mathbf{a}_r(\mu_z^r) \otimes \mathbf{a}_t(\mu_z^t) \otimes \mathbf{a}_d(\gamma_z) \otimes \mathbf{a}_\tau(\eta_z))$ with

$$\begin{aligned} \mathbf{a}_d(\gamma_z) &= [1 \quad \exp(j\gamma_z) \quad \cdots \quad \exp(j(R-1)\gamma_z)]^T \\ \mathbf{a}_\tau(\eta_z) &= [1 \quad \exp(-j\eta_z) \quad \cdots \quad \exp(-j(U-1)\eta_z)]^T \end{aligned} \quad (18)$$

Defining $\alpha_z(i) = \beta_z \exp(-j(i-1)\eta_z)$, (17) can be expressed as

$$\begin{aligned} \mathbf{x}_d(i) &= \sum_{z=1}^Z \alpha_z(i) \mathbf{a}(\mu_z^r, \mu_z^t, \gamma_z, \eta_z) \\ &= \mathbf{A}(\boldsymbol{\mu}^r, \boldsymbol{\mu}^t, \boldsymbol{\gamma}, \boldsymbol{\eta}) \boldsymbol{\alpha}(i) \end{aligned} \quad (19)$$

where $\boldsymbol{\alpha}(i) = [\alpha_1 \quad \cdots \quad \alpha_Z] \in \mathbb{C}^{Z \times 1}$ and $\mathbf{A} = [\mathbf{a}(\mu_1^r, \mu_1^t, \gamma_1, \eta_1) \quad \cdots \quad \mathbf{a}(\mu_Z^r, \mu_Z^t, \gamma_Z, \eta_Z)]$ is a Vandermonde structured steering matrix, with $\boldsymbol{\mu}^r, \boldsymbol{\mu}^t, \boldsymbol{\gamma}, \boldsymbol{\eta}$ defined as $Z \times 1$ vectors of their respective parameters. Clearly, (17) corresponds to a four dimensional array data model obtained by combining the transmit spatial, temporal, frequency and receive spatial dimensions of the wideband MIMO channel. A summary of the dimensions and corresponding parameters is shown in Table II.

B. TSS Transformation

As shown in (10) and Table I, parametrizing the TSSM requires $3Z$ structural parameters $\{\mu_z^r, \gamma_z, \eta_z\}_{z=1}^Z$. We will here derive a data structure that allows joint extraction of these parameters from (10). Using the Q temporal samples, we start by forming a block Hankel matrix for each frequency sample,

$$\mathbf{B}_k = \begin{bmatrix} \mathbf{H}(1, k) & \mathbf{H}(2, k) & \cdots & \mathbf{H}(R, k) \\ \mathbf{H}(2, k) & \mathbf{H}(3, k) & \cdots & \mathbf{H}(R+1, k) \\ \vdots & \vdots & \ddots & \vdots \\ \mathbf{H}(S, k) & \mathbf{H}(S+1, k) & \cdots & \mathbf{H}(Q, k) \end{bmatrix} \quad (20)$$

Note that (20) combines the receive spatial and temporal property of the channel into one dimension corresponding

to the columns of \mathbf{B}_k . In order to include the frequency dimension of the wideband channel, we form another block Hankel matrix from (20) as

$$\mathbf{X}_t = \begin{bmatrix} \mathbf{B}_1 & \mathbf{B}_2 & \cdots & \mathbf{B}_T \\ \mathbf{B}_2 & \mathbf{B}_3 & \cdots & \mathbf{B}_{T+1} \\ \vdots & \vdots & \ddots & \vdots \\ \mathbf{B}_U & \mathbf{B}_{U+1} & \cdots & \mathbf{B}_K \end{bmatrix} \quad (21)$$

Based on the transformations in (20) and (21), the data in the columns of \mathbf{X}_t is given by

$$\mathbf{x}_t(i) = \mathbf{A}(\boldsymbol{\mu}^r, \boldsymbol{\gamma}, \boldsymbol{\eta}) \boldsymbol{\alpha}(i) \quad (22)$$

where $\mathbf{A}(\boldsymbol{\mu}^r, \boldsymbol{\gamma}, \boldsymbol{\eta})$ is defined analogously to (19).³

C. MSS Transformation

The MSSM is parametrized by $2Z$ structural parameters and NMZ complex amplitude parameters. Extraction of these parameters from the channel requires a two-dimensional datum. Similar to (14), we form a Hankel matrix

$$\mathbf{C}_k = \begin{bmatrix} \mathbf{h}^T(1, k) & \mathbf{h}^T(2, k) & \cdots & \mathbf{h}^T(R, k) \\ \mathbf{h}^T(2, k) & \mathbf{h}^T(3, k) & \cdots & \mathbf{h}^T(R+1, k) \\ \vdots & \vdots & \ddots & \vdots \\ \mathbf{h}^T(S, k) & \mathbf{h}^T(S+1, k) & \cdots & \mathbf{h}^T(Q, k) \end{bmatrix} \quad (23)$$

Note that the columns of \mathbf{C}_k correspond to S temporal measurements of the channel and can be modelled as

$$\mathbf{c}_k(i) = \sum_{z=1}^Z \alpha_z(i) \mathbf{a}_d(\gamma_z) \quad (24)$$

where $\mathbf{a}_d(\gamma_z)$ is an S dimensional vector defined in (18). The data in (24) provides information about the Doppler shifts of the channel. The frequency structure of the channel can be included by forming a block Hankel matrix \mathbf{X}_m analogous to \mathbf{X}_d with \mathbf{D}_k replaced with \mathbf{C}_k . The columns of \mathbf{X}_m can be shown using (24) to be

$$\begin{aligned} \mathbf{x}_m(i) &= \sum_{z=1}^Z \alpha_z(i) (\mathbf{a}_d(\gamma_z) \otimes \mathbf{a}_\tau(\eta_z)) \\ &= \mathbf{A}(\boldsymbol{\gamma}, \boldsymbol{\eta}) \boldsymbol{\alpha}(i) \end{aligned} \quad (25)$$

As shown in (25), \mathbf{X}_m corresponds to a two-dimensional datum obtained by combining the temporal and frequency structure of the channel. The Doppler shifts and delays of arrival can therefore be extracted jointly using appropriate parameter estimation algorithms.

IV. PREDICTION ALGORITHMS

We now propose prediction algorithms using the models developed in Section II and the transformed data derived in Section III. We will henceforth refer to the algorithms as WIMEMCHAP: Wideband Multidimensional Esprit based

³For simplicity of notation, we use a common variable for the array steering matrix in all three models. The precise definition is obvious from the context.

Mimo CHannel Predictor, and use the acronyms for the models as prefixes to distinguish the schemes. For example, the algorithm based on TSSM will be called TSSM-WIMEMCHAP and so on. Note that although the algorithms are based on the same idea of parametric modelling, they differ in the model, dimension of parameter estimation and number of amplitude and structural parameters to be estimated.

A. DOD/DOA-WIMEMCHAP

Consider the transformed data model in (17) and (19). Since the array steering matrix \mathbf{A} is equivalent to a product of four Vandermonde matrices, the invariance structure in \mathbf{A} can be utilized to estimate the parameters of the channel. Motivated by the accuracy and computational efficiency of the ESPRIT algorithm [27], we propose an adaptation of multidimensional extension of ESPRIT to jointly extract the parameter sets $\{\mu_z^r, \mu_z^t, \gamma_z, \eta_z\}_{z=1}^Z$ and apply the parameter estimates to extrapolate the channel. The prediction algorithm can be divided into the following stages:

- covariance matrix estimation and subspace separation,
- number of paths estimation,
- joint parameter estimation,
- channel extrapolation.

We will now describe the different stages of the algorithm.

1) *Covariance Matrix Estimation*: In the presence of estimation or measurement noise, the model in (19) becomes

$$\hat{\mathbf{x}}_d(i) = \mathbf{A}(\mu^r, \mu^t, \gamma, \eta)\alpha(i) + \mathbf{n}(i) \quad (26)$$

where $\mathbf{n}(i)$ models the effects of \mathbf{N} in (12). The covariance matrix (containing the spatial, temporal and frequency correlations) can be estimated from (26) as

$$\begin{aligned} \hat{\mathbf{C}}_d &= \frac{1}{RT} \sum_{i=1}^{RT} \hat{\mathbf{x}}_d(i) \hat{\mathbf{x}}_d(i)^H \\ &= \mathbf{A}(\mu^r, \mu^t, \gamma, \eta) \mathbf{C}_{\alpha\alpha} \mathbf{A}(\mu^r, \mu^t, \gamma, \eta)^H + \sigma^2 \mathbf{I} \end{aligned} \quad (27)$$

where $(\cdot)^H$ denotes the Hermitian transpose and $\mathbf{C}_{\alpha\alpha} = \frac{1}{RT} \sum_{i=1}^{RT} \alpha \alpha^H$ is the covariance matrix of the amplitude parameters. $\hat{\mathbf{C}}_d$ can be expressed in terms of $\hat{\mathbf{X}}_d$ in (16) as

$$\hat{\mathbf{C}}_d = \frac{1}{RT} \hat{\mathbf{X}}_d \hat{\mathbf{X}}_d^H \quad (28)$$

2) *Number of Paths Estimation and Subspace Decomposition*: Estimation of the number of paths Z is typically a model order selection problem. The Minimum Description Length (MDL) is often used for this purpose due to its accuracy and consistency [29, 30]. We utilize a modified version of the MDL referred to as the Minimum Mean Square Error (MMSE)-MDL [31] defined as

$$\hat{Z} = \arg \min_{z=1, \dots, N_{MSU}-1} RT \log(\lambda_z) + \frac{1}{2}(z^2 + z) \log RT \quad (29)$$

where λ_z are the eigenvalues of $\hat{\mathbf{C}}_d$. Once \hat{Z} has been estimated, the eigenvalue decomposition of \mathbf{C}_d can be expressed as

$$\begin{aligned} \mathbf{C}_d &= [\mathbf{E}_s \quad \mathbf{E}_n] \begin{bmatrix} \mathbf{\Lambda}_s & \\ & \mathbf{\Lambda}_n \end{bmatrix} \begin{bmatrix} \mathbf{E}_s^H \\ \mathbf{E}_n^H \end{bmatrix} \\ &= \mathbf{E}_s \mathbf{\Lambda}_s \mathbf{E}_s^H + \mathbf{E}_n \mathbf{\Lambda}_n \mathbf{E}_n^H \end{aligned} \quad (30)$$

where \mathbf{E}_s and $\mathbf{\Lambda}_s$ are the signal subspace eigenvectors and the associated eigenvalues, respectively. The noise subspace eigenvectors and eigenvalues are contained in \mathbf{E}_n and $\mathbf{\Lambda}_n$, respectively.

3) *Parameter Estimation*: We now outline the process of obtaining the parameter sets $\{\mu_z^r, \mu_z^t, \gamma_z, \eta_z\}_{z=1}^Z$ in Table I. In order to explore the invariance structure [27] in the Vandermonde structured space-time-frequency manifold matrix, \mathbf{A} , we define the following selection matrices:

$$\begin{aligned} \mathbf{S}_{1\theta} &= [\mathbf{I}_{(N-1)} \quad \mathbf{0}_{(N-1)}] & \mathbf{S}_{\theta 1} &= \mathbf{I}_M \otimes \mathbf{I}_S \otimes \mathbf{I}_U \otimes \mathbf{S}_{1\theta} \\ \mathbf{S}_{2\theta} &= [\mathbf{0}_{(N-1)} \quad \mathbf{I}_{(N-1)}] & \mathbf{S}_{\theta 2} &= \mathbf{I}_M \otimes \mathbf{I}_S \otimes \mathbf{I}_U \otimes \mathbf{S}_{2\theta} \\ \mathbf{S}_{1\phi} &= [\mathbf{I}_{(M-1)} \quad \mathbf{0}_{(M-1)}] & \mathbf{S}_{\phi 1} &= \mathbf{I}_S \otimes \mathbf{I}_U \otimes \mathbf{S}_{1\phi} \otimes \mathbf{I}_N \\ \mathbf{S}_{2\phi} &= [\mathbf{0}_{(M-1)} \quad \mathbf{I}_{(M-1)}] & \mathbf{S}_{\phi 2} &= \mathbf{I}_S \otimes \mathbf{I}_U \otimes \mathbf{J}_{2\phi} \otimes \mathbf{I}_N \\ \mathbf{S}_{1\nu} &= [\mathbf{I}_{(S-1)} \quad \mathbf{0}_{(S-1)}] & \mathbf{S}_{\nu 1} &= \mathbf{I}_U \otimes \mathbf{S}_{1\nu} \otimes \mathbf{I}_N \otimes \mathbf{I}_M \\ \mathbf{S}_{2\nu} &= [\mathbf{0}_{(S-1)} \quad \mathbf{I}_{(S-1)}] & \mathbf{S}_{\nu 2} &= \mathbf{I}_U \otimes \mathbf{S}_{2\nu} \otimes \mathbf{I}_N \otimes \mathbf{I}_M \\ \mathbf{S}_{1\tau} &= [\mathbf{I}_{(U-1)} \quad \mathbf{0}_{(U-1)}] & \mathbf{S}_{\tau 1} &= \mathbf{S}_{1\tau} \otimes \mathbf{I}_N \otimes \mathbf{I}_M \otimes \mathbf{I}_S \\ \mathbf{S}_{2\tau} &= [\mathbf{0}_{(U-1)} \quad \mathbf{I}_{(U-1)}] & \mathbf{S}_{\tau 2} &= \mathbf{S}_{2\tau} \otimes \mathbf{I}_N \otimes \mathbf{I}_M \otimes \mathbf{I}_S \end{aligned} \quad (31)$$

where \mathbf{I}_F is an $F \times F$ identity matrix and $\mathbf{0}_F \in \mathbf{R}^F$ is an F -dimensional vector of zeros. Using the selection matrices in (31), we define the following invariance equations

$$\begin{aligned} \mathbf{S}_{\theta 2} \mathbf{E}_s &= \mathbf{S}_{\theta 1} \mathbf{E}_s \Phi_r & \mathbf{S}_{\phi 2} \mathbf{E}_s &= \mathbf{S}_{\phi 1} \mathbf{E}_s \Phi_t \\ \mathbf{S}_{\nu 2} \mathbf{E}_s &= \mathbf{S}_{\nu 1} \mathbf{E}_s \Phi_d & \mathbf{S}_{\tau 2} \mathbf{E}_s &= \mathbf{S}_{\tau 1} \mathbf{E}_s \Phi_f \end{aligned} \quad (32)$$

where Φ_r , Φ_t , Φ_d and Φ_f are matrices, the eigenvalues of which contain information about the parameters:

$$\begin{aligned} \text{eig}(\Phi_r) &= \text{diag} [\exp(j\mu_1^r), \exp(j\mu_2^r), \dots, \exp(j\mu_Z^r)] \\ \text{eig}(\Phi_t) &= \text{diag} [\exp(j\mu_1^t), \exp(j\mu_2^t), \dots, \exp(j\mu_Z^t)] \\ \text{eig}(\Phi_d) &= \text{diag} [\exp(j\gamma_1), \exp(j\gamma_2), \dots, \exp(j\gamma_Z)] \\ \text{eig}(\Phi_f) &= \text{diag} [\exp(j\eta_1), \exp(j\eta_2), \dots, \exp(j\eta_Z)] \end{aligned} \quad (33)$$

where $\text{eig}(\cdot)$ denotes the diagonal eigenvalue matrix of the associated matrix. We minimize the squared error of the equations in (32) to obtain

$$\Phi_r = ((\mathbf{S}_{\theta 2} \mathbf{E}_s)^H (\mathbf{S}_{\theta 2} \mathbf{E}_s))^{-1} (\mathbf{S}_{\theta 2} \mathbf{E}_s)^H (\mathbf{S}_{\theta 1} \mathbf{E}_s) \quad (34)$$

$$\Phi_t = ((\mathbf{S}_{\phi 2} \mathbf{E}_s)^H (\mathbf{S}_{\phi 2} \mathbf{E}_s))^{-1} (\mathbf{S}_{\phi 2} \mathbf{E}_s)^H (\mathbf{S}_{\phi 1} \mathbf{E}_s) \quad (35)$$

$$\Phi_d = ((\mathbf{S}_{\nu 2} \mathbf{E}_s)^H (\mathbf{S}_{\nu 2} \mathbf{E}_s))^{-1} (\mathbf{S}_{\nu 2} \mathbf{E}_s)^H (\mathbf{S}_{\nu 1} \mathbf{E}_s) \quad (36)$$

$$\Phi_f = ((\mathbf{S}_{\tau 2} \mathbf{E}_s)^H (\mathbf{S}_{\tau 2} \mathbf{E}_s))^{-1} (\mathbf{S}_{\tau 2} \mathbf{E}_s)^H (\mathbf{S}_{\tau 1} \mathbf{E}_s) \quad (37)$$

Estimates of the AOAs, AODs, Doppler shifts and delays could be obtained directly from the solutions of (34)–(37) followed by an additional pairing stage. In order to achieve automatic pairing of the estimates, we utilize a scheme similar to the mean eigenvalue decomposition (MEVD) pairing scheme [32]. Defining

$$\Upsilon = \Phi_r + \Phi_t + \Phi_d + \Phi_f \quad (38)$$

we perform eigenvalue decomposition of Υ to obtain the common eigenvectors of the four matrices in the sum

$$\Upsilon = \Sigma \Lambda \Sigma^{-1} \quad (39)$$

The diagonal eigenvalue matrices are then obtained using

$$\Xi_\theta = \Sigma^{-1} \Phi_r \Sigma \quad (40)$$

$$\Xi_\phi = \Sigma^{-1} \Phi_t \Sigma \quad (41)$$

$$\Xi_\nu = \Sigma^{-1} \Phi_d \Sigma \quad (42)$$

$$\Xi_\tau = \Sigma^{-1} \Phi_f \Sigma \quad (43)$$

where $\Xi_\theta = \text{eig}(\Phi_r)$, $\Xi_\phi = \text{eig}(\Phi_t)$, $\Xi_\nu = \text{eig}(\Phi_d)$ and $\Xi_\tau = \text{eig}(\Phi_f)$. Finally, estimates of the parameters are evaluated from (33) as

$$\hat{\mu}^r = -\arg(\text{diag}(\Xi_\theta)) \quad (44)$$

$$\hat{\gamma} = \arg(\text{diag}(\Xi_\nu)) \quad (45)$$

$$\hat{\mu}^t = -\arg(\text{diag}(\Xi_\phi)) \quad (46)$$

$$\hat{\eta} = -\arg(\text{diag}(\Xi_\tau)) \quad (47)$$

4) *Complex Amplitude Estimation*: We assume that the complex amplitude of each path is equal for all antenna pairs, which is reasonable considering the separation of gain β_z from array dependent steering vectors \mathbf{a}_r and \mathbf{a}_t in (6). The complex amplitudes can therefore be estimated via a least square fit to the known channel. Using the Vandermonde structure of \mathbf{A} and (6), we form the following equation for the first entry of $\hat{\mathbf{H}}$ in (12) for the first subcarrier

$$\begin{bmatrix} \hat{h}_{11}(1) \\ \hat{h}_{11}(2) \\ \vdots \\ \hat{h}_{11}(Q) \end{bmatrix} = \begin{bmatrix} 1 & \cdots & 1 \\ e^{j\hat{\gamma}_1} & \cdots & e^{j\hat{\gamma}_Z} \\ \vdots & \ddots & \vdots \\ e^{j(Q-1)\hat{\gamma}_1} & \cdots & e^{j(Q-1)\hat{\gamma}_Z} \end{bmatrix} \begin{bmatrix} \beta_1 \\ \beta_2 \\ \vdots \\ \beta_Z \end{bmatrix} + \begin{bmatrix} n(1) \\ n(2) \\ \vdots \\ n(Q) \end{bmatrix} \quad (48)$$

which can be written in matrix form as

$$\hat{\mathbf{h}}_{11} = \hat{\mathbf{W}}\boldsymbol{\beta} + \mathbf{n} \quad (49)$$

$\boldsymbol{\beta}$ can be obtained via a regularized LS solution of (49) as

$$\hat{\boldsymbol{\beta}} = (\hat{\mathbf{W}}^H \hat{\mathbf{W}} + \sigma \mathbf{I}) \hat{\mathbf{W}}^H \hat{\mathbf{h}}_{11} \quad (50)$$

where σ is the regularization parameter chosen to minimize the effects of errors in $\hat{\mathbf{W}}$ on the estimation. For the rest of this paper σ is chosen empirically as 10^{-5} . Note that although (50) gives an estimate of the complex amplitudes, our preliminary simulations show that improved estimates can be obtained by using more entries of $\hat{\mathbf{H}}$ in the estimation. We therefore generalize (49) as

$$\hat{\mathbf{h}}_{nm} = \hat{\mathbf{W}}_{nm} \boldsymbol{\beta} + \mathbf{n} \quad \forall n \in [1, N] \quad m \in [1, M] \quad (51)$$

with $\hat{\mathbf{W}}_{nm}$ defined as

$$\hat{\mathbf{W}}_{nm} = \mathbf{v}_n^r \diamond \hat{\mathbf{W}} \diamond \mathbf{v}_m^t \quad (52)$$

where \diamond denotes the Khatri-Rao product, and \mathbf{v}_n^r is defined as

$$\mathbf{v}_n^r = \begin{bmatrix} e^{j(n-1)\mu_1^r} & e^{j(n-1)\mu_2^r} & \cdots & e^{j(n-1)\mu_Z^r} \end{bmatrix} \quad (53)$$

\mathbf{v}_m^t is defined analogously. We combine the NM equations in (51) and solve for $\hat{\boldsymbol{\beta}}$ as

$$\hat{\boldsymbol{\beta}} = (\hat{\mathbf{W}}_D^H \hat{\mathbf{W}}_D + \sigma \mathbf{I}) \hat{\mathbf{W}}_D^H \hat{\mathbf{h}} \quad (54)$$

where $\hat{\mathbf{h}} = \begin{bmatrix} \hat{\mathbf{h}}_{11}^T & \hat{\mathbf{h}}_{12} & \cdots & \hat{\mathbf{h}}_{NM} \end{bmatrix}$ and $\hat{\mathbf{W}}_D = \begin{bmatrix} \hat{\mathbf{W}}_{11} & \hat{\mathbf{W}}_{12} & \cdots & \hat{\mathbf{W}}_{NM} \end{bmatrix}^T$. It should be noted that the choice of using (50) or (54) is essentially a compromise between complexity and accuracy, since the improved amplitude estimates in (54) is achieved at the cost of increased computational complexity. We will utilize (54) for our analysis in this paper.

5) *Channel Prediction*: Once the parameters of the model have been estimated, the time-varying frequency selective channel is predicted via

$$\hat{\mathbf{H}}(q, k) = \sum_{z=1}^{\hat{Z}} \hat{\beta}_z \mathbf{a}_r(\hat{\mu}_z^r) \mathbf{a}_t^T(\hat{\mu}_z^t) \exp(jq\hat{\gamma}_z - jk\hat{\eta}_z) \quad (55)$$

B. TSSM-WIMEMCHAP

Unlike the DOD/DOA-WIMEMCHAP approach, the TSSM-WIMEMCHAP involves 3D parameter estimation. The steps involved in the TSSM-WIMEMCHAP approach are as follow.

1) *Covariance Matrix Estimation*: The covariance matrix, containing the receive spatial, temporal and frequency correlations, is estimated from (21) as

$$\mathbf{C}_t = \frac{1}{MRT} \hat{\mathbf{X}}_t \hat{\mathbf{X}}_t^H \quad (56)$$

2) *Number of Paths Estimation and Subspace Decomposition*: We again estimate Z using the MMSE-MDL criterion in (29) and eigendecompose \mathbf{C}_t as

$$\mathbf{C}_t = \mathbf{E}_s \Lambda_s \mathbf{E}_s^H + \mathbf{E}_n \Lambda_n \mathbf{E}_n^H \quad (57)$$

3) *Parameter Estimation*: Extraction of the parameter sets $\{\mu_z^r, \gamma_z, \eta_z\}_{z=1}^{\hat{Z}}$ requires a 3D estimation procedure. Similar to (31), we form the following 3D selection matrices

$$\begin{aligned} \mathbf{S}_{\theta 1} &= \mathbf{I}_S \otimes \mathbf{I}_U \otimes \mathbf{S}_{1\theta} \\ \mathbf{S}_{\theta 2} &= \mathbf{I}_S \otimes \mathbf{I}_U \otimes \mathbf{S}_{2\theta} \\ \mathbf{S}_{\gamma 1} &= \mathbf{I}_S \otimes \mathbf{S}_{1\gamma} \otimes \mathbf{I}_N \\ \mathbf{S}_{\gamma 2} &= \mathbf{I}_S \otimes \mathbf{S}_{2\gamma} \otimes \mathbf{I}_N \\ \mathbf{S}_{\eta 1} &= \mathbf{S}_{1\eta} \otimes \mathbf{I}_U \otimes \mathbf{I}_N \\ \mathbf{S}_{\eta 2} &= \mathbf{S}_{2\eta} \otimes \mathbf{I}_U \otimes \mathbf{I}_N \end{aligned} \quad (58)$$

Using the selection matrices in (58), we form 3D invariance equations analogous to (32) and solve (35)–(37), (38), (39), (41)–(43) and (45)–(47) to obtain the parameter estimates.

4) *TSS Estimation*: The TSS can be similarly obtained via a least square approach. We assume that the TSS of the scattering sources are equal for all subcarriers and use the channel for the first subcarrier in the estimation⁴. Let $\mathbf{s}^m = [\mathbf{s}_1(m) \quad \mathbf{s}_2(m) \quad \cdots \quad \mathbf{s}_{\hat{Z}}(m)]^T$ be a vector containing the m th entry of the TSS for all paths. Using (10), we obtain

$$\hat{\mathbf{h}}_m = \hat{\mathbf{W}}_m \mathbf{s}^m + \mathbf{n} \quad \forall m \in [1, M] \quad (59)$$

⁴The accuracy of the TSS estimation may be improved by incorporating all subcarriers. However, the computational complexity will scale with the number of subcarriers.

where $\hat{\mathbf{h}}_m = [\hat{h}_{1m}(1), \hat{h}_{1m}(2), \dots, \hat{h}_{1m}(Q), \dots, \hat{h}_{Nm}(Q)]^T$ and $\hat{\mathbf{W}}_m$ is defined as

$$\hat{\mathbf{W}}_m = \mathbf{A}_r \diamond \hat{\mathbf{W}} \quad (60)$$

where \mathbf{A}_r is the receive array steering matrix defined for the ULA as

$$\mathbf{A}_r = [\mathbf{a}(\mu_1^r), \mathbf{a}(\mu_2^r), \dots, \mathbf{a}(\mu_Z^r)] \\ = \begin{bmatrix} 1 & 1 & \dots & 1 \\ e^{j\mu_1^r} & e^{j\mu_2^r} & \dots & e^{j\mu_Z^r} \\ \vdots & \vdots & \ddots & \vdots \\ e^{j(N-1)\mu_1^r} & e^{j(N-1)\mu_2^r} & \dots & e^{j(N-1)\mu_Z^r} \end{bmatrix} \quad (61)$$

We solve (59) using the least square approach and estimate the TSS for each path as

$$\hat{\mathbf{s}}_z = [\hat{\mathbf{s}}^1(z) \quad \hat{\mathbf{s}}^2(z) \quad \dots \quad \hat{\mathbf{s}}^M(z)]^T \quad (62)$$

5) *Channel Prediction*: Extrapolation of the channel using the TSSM-WIMEMCHAP is obtained from

$$\tilde{\mathbf{H}}(q, k) = \sum_{z=1}^{\hat{Z}} \mathbf{a}_r(\hat{\mu}_z^r) \hat{\mathbf{s}}_z^T \exp(jq\hat{\gamma}_z - jk\hat{\eta}_z) \quad (63)$$

C. MSSM-WIMEMCHAP

This approach involves estimation of the Doppler shifts and delays, which can be achieved via a 2D estimation procedure. This method is essentially an extension of the SISO schemes in [15] to MIMO channels. A summary of the steps in the prediction is given below.

1) *Covariance Matrix Estimation*: The time-frequency covariance matrix is estimated using

$$\mathbf{C}_m = \frac{1}{NMRT} \hat{\mathbf{X}}_m \hat{\mathbf{X}}_m^H \quad (64)$$

2) *Number of Paths Estimation and Subspace Decomposition*: We estimate the number of paths using the MMSE-MDL criterion in (29) with the eigenvalues of \mathbf{C}_M . The eigendecomposition of \mathbf{C}_M can thus be expressed as

$$\mathbf{C}_M = \mathbf{E}_s \Lambda_s \mathbf{E}_s^H + \mathbf{E}_n \Lambda_n \mathbf{E}_n^H \quad (65)$$

3) *Parameter Estimation*: Extraction of the parameter sets $\{\gamma_z, \eta_z\}_{z=1}^{\hat{Z}}$ requires 2D estimation and four selection matrices defined as

$$\begin{aligned} \mathbf{S}_{\gamma 1} &= \mathbf{I}_U \otimes \mathbf{S}_{1\gamma} \\ \mathbf{S}_{\gamma 2} &= \mathbf{I}_U \otimes \mathbf{S}_{2\gamma} \\ \mathbf{S}_{\eta 1} &= \mathbf{S}_{1\eta} \otimes \mathbf{I}_S \\ \mathbf{S}_{\eta 2} &= \mathbf{S}_{2\eta} \otimes \mathbf{I}_S \end{aligned} \quad (66)$$

We solve (36)–(37), (38)–(39), (42)–(43) and (46)–(47) to obtain the parameter estimates.

4) *MSS Estimation*: Let $\mathbf{s}_{nm} = [\mathbf{S}_1(n, m) \quad \mathbf{S}_2(n, m) \quad \dots \quad \mathbf{S}_Z(n, m)]^T \in \mathbb{C}^{Z \times 1}$ be a vector containing the (n, m) th entry of the MSS for all paths. Using (11), it can be easily shown that

$$\hat{\mathbf{h}}_{nm} = \hat{\mathbf{W}}_{11} \mathbf{s}_{nm} + \mathbf{n} \quad (67)$$

for $n \in [1, N]$ and $m \in [1, M]$. We find the least square solution $\hat{\mathbf{s}}_{nm}$ to (67) for all antenna pairs and compute the MSS for the z th path as

$$\hat{\mathbf{S}}_z = \begin{bmatrix} \hat{\mathbf{s}}_{11}(z) & \hat{\mathbf{s}}_{12}(z) & \dots & \hat{\mathbf{s}}_{1M}(z) \\ \hat{\mathbf{s}}_{21}(z) & \hat{\mathbf{s}}_{22}(z) & \dots & \hat{\mathbf{s}}_{2M}(z) \\ \vdots & \vdots & \ddots & \vdots \\ \hat{\mathbf{s}}_{N1}(z) & \hat{\mathbf{s}}_{N2}(z) & \dots & \hat{\mathbf{s}}_{NM}(z) \end{bmatrix} \quad (68)$$

5) *Channel Prediction*: Channel prediction using the MSSM-WIMEMCHAP is achieved using

$$\tilde{\mathbf{H}}(q, k) = \sum_{z=1}^{\hat{Z}} \hat{\mathbf{S}}_z^T \exp(jq\hat{\gamma}_z - jk\hat{\eta}_z) \quad (69)$$

V. PERFORMANCE BOUNDS

A commonly used bound on the performance of an unbiased estimator is the Cramer-Rao lower bound (CRLB) [33]. In this section, we derive the bound on the variance of prediction error in wideband MIMO systems. While similar results have been presented in [20, 26], we present an alternative, simpler formulation. Consider the vectorized model in (13). Using the properties of Kronecker products, $\mathbf{h}(q, k)$ can be written as

$$\mathbf{h}(q, k) = (\mathbf{A}_r \diamond \mathbf{A}_t) \boldsymbol{\alpha}(q, k) \quad (70)$$

where

$$\boldsymbol{\alpha}(q, k) = [\beta_1 \exp(jq\gamma_1 - jk\eta_1) \quad \dots \quad \beta_Z \exp(jq\gamma_Z - jk\eta_Z)] \quad (71)$$

and \mathbf{A}_r is the receive array steering matrix in (61). The transmit array response matrix, \mathbf{A}_t is defined analogously by replacing μ_z^r with μ_z^t . We arrange the QK known samples into the vector

$$\mathbf{h} = [\mathbf{h}^T(1, 1), \dots, \mathbf{h}^T(Q, 1), \mathbf{h}^T(1, 2), \dots, \mathbf{h}^T(Q, 2), \dots, \mathbf{h}^T(1, K), \dots, \mathbf{h}^T(Q, K)] \quad (72)$$

and define Vandermonde matrices \mathbf{A}_d and \mathbf{A}_f as

$$\mathbf{A}_d = \begin{bmatrix} 1 & \dots & 1 \\ \exp(j\gamma_1) & \dots & \exp(j\gamma_Z) \\ \vdots & \ddots & \vdots \\ \exp(j(Q-1)\gamma_1) & \dots & \exp(j(Q-1)\gamma_Z) \end{bmatrix} \quad (73)$$

and

$$\mathbf{A}_f = \begin{bmatrix} 1 & \dots & 1 \\ \exp(-j\eta_1) & \dots & \exp(-j\eta_Z) \\ \vdots & \ddots & \vdots \\ \exp(-j(K-1)\eta_1) & \dots & \exp(-j(K-1)\eta_Z) \end{bmatrix} \quad (74)$$

It can easily be verified that

$$\begin{aligned}\mathbf{h} &= (\mathbf{A}_r \diamond \mathbf{A}_t \diamond \mathbf{A}_d \diamond \mathbf{A}_f) \boldsymbol{\beta} \\ &= \mathbf{A} \boldsymbol{\beta}\end{aligned}\quad (75)$$

where $\mathbf{A} = (\mathbf{A}_r \diamond \mathbf{A}_t \diamond \mathbf{A}_d \diamond \mathbf{A}_f)$. Let the parameterization of the channel be denoted by

$$\boldsymbol{\Theta} = [\sigma^2, \boldsymbol{\theta}^T, \boldsymbol{\phi}^T, \boldsymbol{\gamma}^T, \boldsymbol{\eta}^T, \Re(\boldsymbol{\beta}^T), \Im(\boldsymbol{\beta}^T)]^T \quad (76)$$

It should be noted that our channel models represent continuous non-linear functions of the parameters and the bound on estimation/prediction of $\mathbf{h}(q, k)$ can be found using the vector formulation of the Cramer–Rao bound for function of parameters. The prediction error can therefore be bounded by [33]

$$\begin{aligned}\mathbf{C}_e(q, k) &= \mathbb{E}[(\hat{\mathbf{h}}(q, k) - \mathbf{h}(q, k))(\hat{\mathbf{h}}(q, k) - \mathbf{h}(q, k))^H] \\ &\geq \frac{\partial \mathbf{h}(q, k)}{\partial \boldsymbol{\Theta}}^H \mathfrak{F}^{-1}(\boldsymbol{\Theta}) \frac{\partial \mathbf{h}(q, k)}{\partial \boldsymbol{\Theta}}\end{aligned}\quad (77)$$

where $\mathfrak{F}^{-1}(\boldsymbol{\Theta})$ is the lower bound on the estimation of channel parameters, and $\mathfrak{F}(\boldsymbol{\Theta})$ is the Fisher information matrix (FIM), calculated using Bangs formula [33]

$$[\mathfrak{F}(\boldsymbol{\Theta})]_{ij} = \text{Tr} \left[\mathbf{C}^{-1} \frac{\partial \mathbf{C}}{\partial \boldsymbol{\Theta}_i} \mathbf{C}^{-1} \frac{\partial \mathbf{C}}{\partial \boldsymbol{\Theta}_j} \right] + 2\Re \left[\frac{\partial \mathbf{h}^H}{\partial \boldsymbol{\Theta}_i} \mathbf{C}^{-1} \frac{\partial \mathbf{h}}{\partial \boldsymbol{\Theta}_j} \right] \quad (78)$$

After evaluating the derivatives and performing straightforward but tedious simplifications, $\mathfrak{F}(\boldsymbol{\Theta})$ is obtained as

$$\mathfrak{F}(\boldsymbol{\Theta}) = \begin{bmatrix} \frac{KQNM}{\sigma^4} & \mathbf{0} \\ \mathbf{0}^T & \mathbf{J}(\boldsymbol{\Theta}) \end{bmatrix} \quad (79)$$

with the Fisher information submatrix defined as

$$\begin{aligned}[\mathbf{J}(\boldsymbol{\Theta})] &= \frac{2}{\sigma^2} \Re \left[(\mathbf{G}_5^H \mathbf{G}_5) \odot (\mathbf{G}_4^H \mathbf{G}_4) \odot (\mathbf{G}_3^H \mathbf{G}_3) \right. \\ &\quad \left. \odot (\mathbf{G}_2^H \mathbf{G}_2) \odot (\mathbf{G}_1^H \mathbf{G}_1) \right]\end{aligned}\quad (80)$$

where \odot denotes the Hardamad product and \mathbf{G}_1 – \mathbf{G}_5 are defined as

$$\mathbf{G}_1 = [\boldsymbol{\alpha}^T \quad \boldsymbol{\alpha}^T \quad \boldsymbol{\alpha}^T \quad \boldsymbol{\alpha}^T \quad \mathbf{1}^T \quad j\mathbf{1}^T] \quad (81)$$

$$\mathbf{G}_2 = [\mathbf{D}_r \quad \mathbf{A}_r \quad \mathbf{A}_r \quad \mathbf{A}_r \quad \mathbf{A}_r \quad \mathbf{A}_r] \quad (82)$$

$$\mathbf{G}_3 = [\mathbf{A}_t \quad \mathbf{D}_t \quad \mathbf{A}_t \quad \mathbf{A}_t \quad \mathbf{A}_t \quad \mathbf{A}_t] \quad (83)$$

$$\mathbf{G}_4 = [\mathbf{A}_d \quad \mathbf{A}_d \quad \mathbf{D}_d \quad \mathbf{A}_d \quad \mathbf{A}_d \quad \mathbf{A}_d] \quad (84)$$

$$\mathbf{G}_5 = [\mathbf{A}_f \quad \mathbf{A}_f \quad \mathbf{A}_f \quad \mathbf{D}_f \quad \mathbf{A}_f \quad \mathbf{A}_f] \quad (85)$$

The matrix $\mathbf{D}_r \in \mathbb{C}^{N \times Z}$ is given by

$$\begin{aligned}\mathbf{D}_r &= \begin{bmatrix} \frac{\partial \mathbf{a}_r(\mu_1^r)}{\partial \mu_1^r} & \cdots & \frac{\partial \mathbf{a}_r(\mu_Z^r)}{\partial \mu_Z^r} \end{bmatrix} \\ &= -j\mathbf{Z}_N \mathbf{A}_r\end{aligned}\quad (86)$$

where \mathbf{Z}_k is a diagonal matrix

$$\mathbf{Z}_k = \begin{bmatrix} 0 & 0 & 0 & \cdots & 0 \\ 0 & 1 & 0 & \cdots & 0 \\ 0 & 0 & 2 & \cdots & 0 \\ \vdots & \vdots & \vdots & \ddots & \vdots \\ 0 & 0 & 0 & \cdots & k-1 \end{bmatrix} \quad (87)$$

\mathbf{D}_t , \mathbf{D}_d and \mathbf{D}_f are defined analogously to (86). Details of the derivations can be found in the Appendix.

VI. NUMERICAL SIMULATIONS

In this section, we evaluate the performance of the proposed schemes. After describing the performance metrics and simulation parameters, we evaluate the the parameter estimation accuracy, followed by the overall prediction performance.

A. Performance Metrics

The overall performance of the prediction schemes is evaluated using Monte Carlo simulations with synthetic data and compared with prediction error bounds in Section V. The normalized mean square error (NMSE) is used as the performance metric. We first define the normalized square error (NSE) over a single realization of the channel as

$$\text{NSE}(q, k) = \frac{\|\tilde{\mathbf{H}}(q, k) - \mathbf{H}(q, k)\|_F^2}{\mathbb{E}[\|\mathbf{H}(q, k)\|_F^2]} \quad (88)$$

where $\|\cdot\|_F$ denotes the Frobenious norm of the associated matrix. The expectation in (88) is approximated over the available temporal and frequency samples.

The performance of the parameter estimation stage is evaluated in terms of the root mean square error (RMSE) defined, for a generic variable x , as

$$\text{RMSE}(\hat{x}) = \sqrt{\frac{1}{N_c} \sum_{c=1}^{N_c} (x - \hat{x}_c)^2} \quad (89)$$

where N_c denotes the number of channel and/or noise realizations and \hat{x}_c is the estimate of x during the c th realization. The NMSE and RMSE are obtained by averaging (88) and (89) over 500 realizations of the channel and/or noise. The RMSE is compared with the square root of the CRB (i.e., diagonal entries of the inverse of (80)).

B. Simulation Parameters

We consider a MIMO–OFDM system with bandwidth $B = 20$ MHz, $N_{\text{sc}} = 1024$ subcarriers including $K = 64$ equally spaced pilot subcarriers. The transmit and receive antenna arrays are both 2-element arrays with inter-antenna spacing $d_r = d_t = \lambda/2$. We consider a carrier frequency of $f_c = 2.1$ GHz and mobile velocity of $v = 50$ km/h. Except where otherwise stated, we use 50 samples at a sampling rate of $10/\lambda$. We consider two methods of generating the channel parameters $\beta_z, \theta_z, \phi_z, \nu_z$. In simulation Scenario I, these are fixed to values given in Table III for all realizations of \mathbf{H} in (6). In simulation Scenario II, they are randomly generated for each channel realization. The amplitudes are generated as complex Gaussian distributed random variables, $\beta_z \sim \mathcal{CN}(0, 1)$. The angles of arrival and departure are assumed to be uniformly distributed, i.e., $\theta_z, \phi_z \sim \mathcal{U}[-\pi, \pi]$. In both cases, the path delays are selected from the Urban macro (UMA) scenario in the WINNER II/3GPP channel [34], given in Table III. Unless otherwise stated, we consider a 6-path channel with parameters in Table III and the error is averaged over 500 noise realizations. .

TABLE III: Propagation Channel Parameters (Scenario I)

Path	Parameters				
	β_z	θ_z	ϕ_z	τ_z (ns)	ν_z (rad/s)
1	-0.76+0.074j	0.49	-2.90	0	185.10
2	-0.76+0.30j	-1.89	0.99	60	-462.10
3	-1.41+0.14j	-2.48	2.99	75	497.31
4	0.16-1.15j	-1.88	1.46	145	-331.90
5	0.37-0.82j	-2.66	2.05	150	208.61
6	-0.33+1.04j	-0.02	-1.60	155	-156.92

C. Parameter Estimation Performance

Since Doppler frequency and delay estimation are part of all the methods, we present results showing the accuracy of their estimates in each algorithm. Figure 1 presents the RMSE of Doppler estimates versus SNR with 50 and 100 known samples of the channel. We observe that the performances of the three methods improves with increasing number of samples and approaches the bound as the SNR increases. Also, we note that the DOD/DOA method outperforms the TSSM and MSSM methods at all SNR values and that the MSSM method yields the highest RMSE. A possible reason for this is the additional channel structure revealed by sampling in a higher number of dimensions. Similar observations are made in Fig. 2, where we plot the RMSE of delay estimates versus SNR.

D. Prediction Performance

We now evaluate the overall prediction performance of the proposed methods. Figures 3–5 correspond to simulation Scenario I. Figure 3 presents the NMSE versus prediction horizon (in wavelengths) at an SNR of 15 dB. The negative values of the prediction horizon correspond to the estimation stage. Again, we observe that the DOD/DOA outperforms TSSM and MSSM methods. In Fig. 4, we plot the corresponding cumulative distribution function (CDF) of the normalized square error (NSE) at a prediction interval of 1λ . The DOD/DOA method has the lowest NSE for all realizations followed by the TSSM. We also observe that utilizing the spatial information in parameter estimation and prediction in the DOD/DOA and TSSM results in a decrease of about 12 dB relative to MSSM.

The effects of increasing SNR on the performance of the proposed schemes is shown in Fig. 5 where we plot the NMSE versus SNR for a prediction horizon of 1λ . As expected, as a consequence of improved parameter estimation, the performance of the algorithms improves with increasing SNR. We observe that the performance of the DOD/DOA and TSSM methods approaches the bound as SNR increases with the DOD/DOA having the lowest NMSE over the entire SNR range considered. This agrees with observations in [26] where it was shown that the prediction error bound obtained from the DOD/DOA model is lower than that for the vector spatial signature model.

We now present results for simulation Scenario II. In Fig. 6, we present the NMSE versus prediction horizon at an SNR of 15 dB. Here, we observe that the averaged performance of all methods degrades when compared to Scenario I. However, the

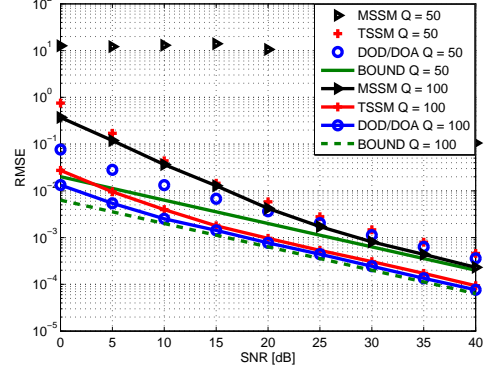


Fig. 1: The RMSE of Doppler frequency estimates versus SNR with [50, 100] known channel samples.

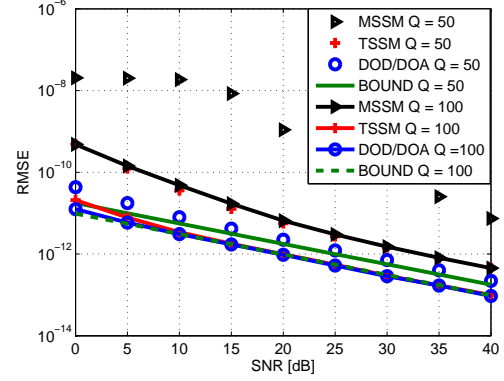


Fig. 2: The RMSE of delay estimates versus SNR with [50, 100] known channel samples.

performance of the DOD/DOA and TSSM schemes are still reasonable with a maximum NMSE of about -12 dB for the TSSM and -22 dB for the DOD/DOA over the 15λ prediction horizon shown. We observe that the MSSM performs poorly with an NMSE of approximately 4.8 dB over the entire region considered. A possible explanation for the increase in NMSE is that unlike in simulation Scenario I, certain channel realizations have parameters which are closer than the resolution limit of the parameter estimation stage, leading to reduced parameter estimation and prediction performance. The CDF of the NSE corresponding to the mean results in Fig. 6 at a prediction interval of 1λ is shown in Fig. 7.

Finally, the CDF of the prediction error of the DOD/DOA for different number of propagation paths is presented in Fig. 8. We observe that the performance of the algorithm degrades with increasing number of paths.

VII. CONCLUSION

We have presented three different parametric schemes for the prediction of mobile MIMO-OFDM channels. The predictors are based on different formulations of the double directional model and original adaptation of multidimensional ESPRIT to jointly extract the channel parameters. Using the vector formulation of Cramer Rao bound for functions of parameters, a simplified form of the lower bound on prediction error

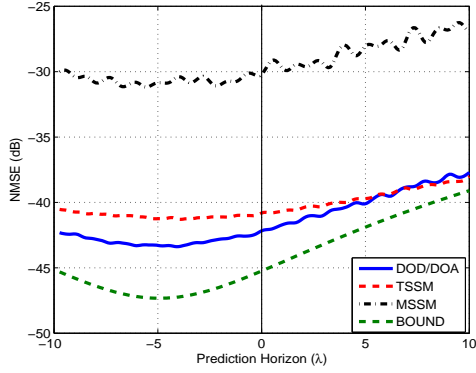


Fig. 3: The averaged NMSE versus prediction horizon for a 2×2 MIMO channel prediction at SNR = 15 dB.

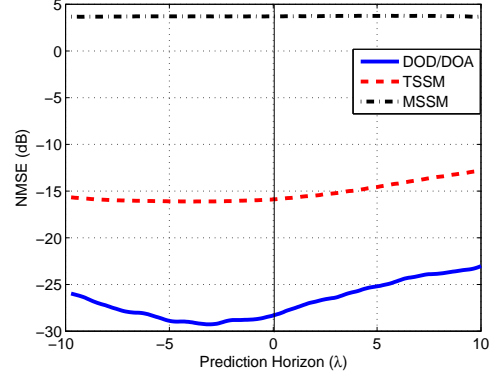


Fig. 6: The averaged NMSE versus prediction horizon for a 2×2 MIMO channel prediction at SNR = 15 dB. Channel and noise are random for each realization. The bound falls outside the plotted range.

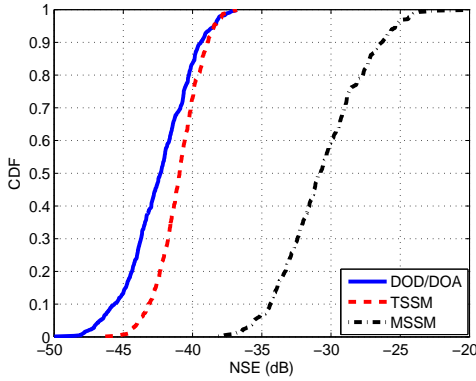


Fig. 4: The cumulative distribution function of NSE for a prediction horizon of 1λ at SNR = 15 dB.

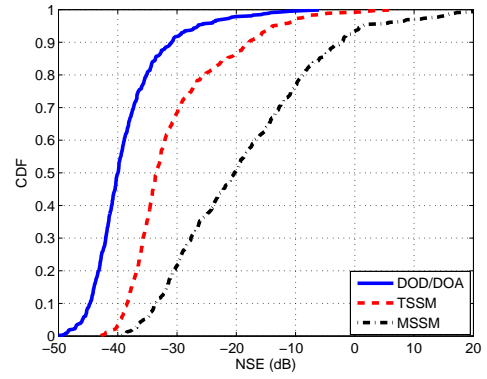


Fig. 7: The cumulative distribution function of NSE for a prediction horizon of 1λ at SNR = 15 dB. Channel and noise are random for each realization.

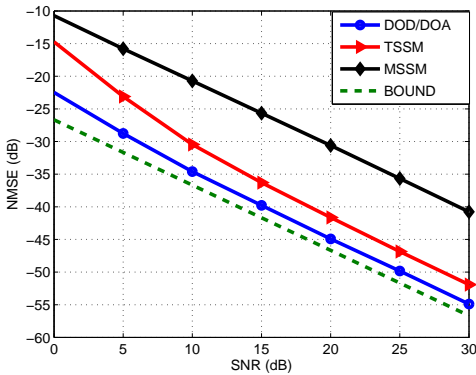


Fig. 5: The averaged NMSE versus SNR for a prediction horizon of 1λ .

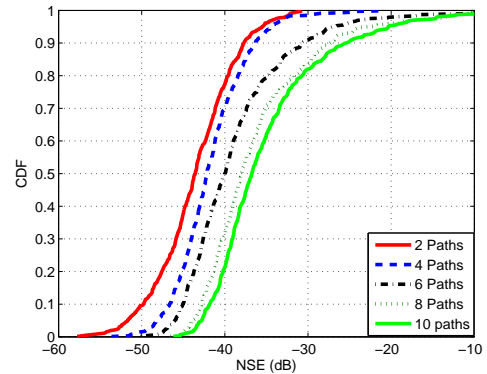


Fig. 8: The cumulative distribution function of NSE for a prediction horizon of 1λ at SNR = 15 dB with $Z = [2, 4, 6, 8, 10]$ paths.

in MIMO-OFDM channel was derived. Numerical simulations indicate that the performance of the algorithms approaches the error bound with increasing SNR and/or number of samples. We have quantified the parameter estimation and channel prediction improvement afforded by the spatial structure of the channel revealed by multiple sampling of the wavefield. The method utilizing both transmit and receive spatial information (DOD/DOA-WIMEMCHAP) outperform those with only receive spatial information (TSSM-WIMEMCHAP) and no spatial information (MSSM-WIMEMCHAP).

APPENDIX A DERIVATIVES FOR THE FIM

In this section, we give the derivatives of the covariance matrix and observation vector \mathbf{h} required for evaluating the FIM expression as given in (80).

A. Derivative with Respect σ^2

Based on the independent Gaussian noise assumption, the derivative of the covariance matrix $\mathbf{C} = \sigma^2 \mathbf{I}$ is

$$\frac{\partial \mathbf{C}}{\partial \sigma^2} = \mathbf{I} \quad (90)$$

On substituting (90) into (78), the entry of the FIM dependent on noise variance is obtained as

$$\text{Tr} \left[\mathbf{C}^{-1} \frac{\partial \mathbf{C}}{\partial \Theta} \mathbf{C}^{-1} \frac{\partial \mathbf{C}}{\partial \Theta} \right] = \frac{KQNM}{\sigma^4} \quad (91)$$

B. Derivative With Respect to $\Re(\beta)$

$$\begin{aligned} \frac{\partial \mathbf{h}}{\partial \Re(\beta_z)} &= \frac{\partial (\mathbf{A}_r \diamond \mathbf{A}_t \diamond \mathbf{A}_d \diamond \mathbf{A}_f) \beta}{\partial \Re(\beta_z)} \\ &= (\mathbf{A}_r \diamond \mathbf{A}_t \diamond \mathbf{A}_d \diamond \mathbf{A}_f) \frac{\partial \beta}{\partial \beta_z} \\ &= (\mathbf{A}_r \diamond \mathbf{A}_t \diamond \mathbf{A}_d \diamond \mathbf{A}_f) \mathbf{\Pi}_z \end{aligned} \quad (92)$$

where $\mathbf{\Pi}_z$ is a $Z \times 1$ vector having a 1 as the z th element and all other elements zero. (92) can further be simplified to

$$\begin{aligned} \frac{\partial \mathbf{h}}{\partial \Re(\beta_z)} &= [\mathbf{A}_r]_{:,z} \otimes [\mathbf{A}_t]_{:,z} \otimes [\mathbf{A}_d]_{:,z} \otimes [\mathbf{A}_f]_{:,z} \\ &= [\mathbf{A}_r \diamond \mathbf{A}_t \diamond \mathbf{A}_d \diamond \mathbf{A}_f]_{:,z} \\ &= [\mathbf{A}]_{:,z} \end{aligned} \quad (93)$$

where $[\mathbf{B}]_{:,z}$ denotes the z th column of \mathbf{B} . Using (93), the derivative with respect to $\Re(\beta)$ is

$$\begin{aligned} \frac{\partial \mathbf{h}}{\partial \Re(\beta)} &= \begin{bmatrix} \frac{\partial \mathbf{h}}{\partial \Re(\beta_1)} & \frac{\partial \mathbf{h}}{\partial \Re(\beta_2)} & \cdots & \frac{\partial \mathbf{h}}{\partial \Re(\beta_Z)} \end{bmatrix} \\ &= [[\mathbf{A}]_{:,1} \quad \cdots \quad [\mathbf{A}]_{:,Z}] \\ &= \mathbf{A} \end{aligned} \quad (94)$$

C. Derivative With Respect to $\Im(\beta)$

$$\begin{aligned} \frac{\partial \mathbf{h}}{\partial \Im(\beta_k)} &= (\mathbf{A}_r \diamond \mathbf{A}_t \diamond \mathbf{A}_d \diamond \mathbf{A}_f) \frac{\partial \beta}{\partial \Im(\beta_z)} \\ &= j(\mathbf{A}_r \diamond \mathbf{A}_t \diamond \mathbf{A}_d \diamond \mathbf{A}_f) \mathbf{\Pi}_z \\ &= j\mathbf{A} \end{aligned} \quad (95)$$

D. Derivative With Respect to μ^r

$$\begin{aligned} \frac{\partial \mathbf{h}}{\partial \mu_z^r} &= \left(\frac{\partial \mathbf{A}_r}{\partial \mu_z^r} \diamond \mathbf{A}_t \diamond \mathbf{A}_d \diamond \mathbf{A}_f \right) \beta \\ &= \left(\frac{\partial [\mathbf{A}_r]_{:,z}}{\partial \mu_z^r} \otimes [\mathbf{A}_t]_{:,z} \otimes [\mathbf{A}_d]_{:,z} \otimes [\mathbf{A}_f]_{:,z} \right) \beta_z \end{aligned} \quad (96)$$

Using (96), we obtain

$$\begin{aligned} \frac{\partial \mathbf{h}}{\partial \mu^r} &= \begin{bmatrix} \frac{\partial \mathbf{h}}{\partial \mu_1^r} & \frac{\partial \mathbf{h}}{\partial \mu_2^r} & \cdots & \frac{\partial \mathbf{h}}{\partial \mu_Z^r} \end{bmatrix} \\ &= \begin{bmatrix} \left(\frac{\partial [\mathbf{A}_r]_{:,1}}{\partial \mu_1^r} \otimes [\mathbf{A}_t]_{:,1} \otimes [\mathbf{A}_d]_{:,1} \otimes [\mathbf{A}_f]_{:,1} \right) \beta_1 & \cdots \\ \left(\frac{\partial [\mathbf{A}_r]_{:,Z}}{\partial \mu_Z^r} \otimes [\mathbf{A}_t]_{:,Z} \otimes [\mathbf{A}_d]_{:,Z} \otimes [\mathbf{A}_f]_{:,Z} \right) \beta_Z \end{bmatrix} \\ &= (\mathbf{D}_r \diamond \mathbf{A}_t \diamond \mathbf{A}_d \diamond \mathbf{A}_f) \mathbf{X} \end{aligned} \quad (97)$$

where

$$\mathbf{D}_r = \begin{bmatrix} \frac{\partial [\mathbf{A}_r]_{:,1}}{\partial \mu_1^r} & \frac{\partial [\mathbf{A}_r]_{:,2}}{\partial \mu_2^r} & \cdots & \frac{\partial [\mathbf{A}_r]_{:,Z}}{\partial \mu_Z^r} \end{bmatrix} \quad (98)$$

and \mathbf{X} is a diagonal matrix with the complex amplitudes β on its diagonal. For the ULA, \mathbf{D}_r can be found using (61) to be

$$\mathbf{D}_r = \begin{bmatrix} 0 & \cdots & 0 \\ j e^{j\mu_1^r} & \cdots & j e^{j\mu_Z^r} \\ 2j e^{j2\mu_1^r} & \cdots & 2j e^{j2\mu_Z^r} \\ \vdots & \ddots & \vdots \\ j(N-1) e^{j(N-1)\mu_1^r} & \cdots & j(N-1) e^{j(N-1)\mu_Z^r} \end{bmatrix} \quad (99)$$

which can be expressed in terms of \mathbf{A}_r as

$$\mathbf{D}_r = j \begin{bmatrix} 0 & 0 & \cdots & 0 \\ 0 & 1 & \cdots & 0 \\ \vdots & \vdots & \ddots & \vdots \\ 0 & 0 & \cdots & (N-1) \end{bmatrix} \mathbf{A}_r \quad (100)$$

E. Derivative With Respect to μ^t

$$\begin{aligned} \frac{\partial \mathbf{h}}{\partial \mu^t} &= \begin{bmatrix} \frac{\partial \mathbf{h}}{\partial \mu_1^t} & \frac{\partial \mathbf{h}}{\partial \mu_2^t} & \cdots & \frac{\partial \mathbf{h}}{\partial \mu_Z^t} \end{bmatrix} \\ &= \begin{bmatrix} \left([\mathbf{A}_r]_{:,1} \otimes \frac{\partial [\mathbf{A}_t]_{:,1}}{\partial \mu_1^t} \otimes [\mathbf{A}_d]_{:,1} \otimes [\mathbf{A}_f]_{:,1} \right) \beta_1 & \cdots \\ \left([\mathbf{A}_r]_{:,Z} \otimes \frac{\partial [\mathbf{A}_t]_{:,Z}}{\partial \mu_Z^t} \otimes [\mathbf{A}_d]_{:,Z} \otimes [\mathbf{A}_f]_{:,Z} \right) \beta_Z \end{bmatrix} \\ &= (\mathbf{A}_r \diamond \mathbf{D}_t \diamond \mathbf{A}_d \diamond \mathbf{A}_f) \mathbf{X} \end{aligned} \quad (101)$$

where \mathbf{D}_t is defined analogous to \mathbf{D}_r .

F. Derivative With Respect to ν

$$\begin{aligned}\frac{\partial \mathbf{h}}{\partial \nu} &= \begin{bmatrix} \frac{\partial \mathbf{h}}{\partial \nu_1} & \frac{\partial \mathbf{h}}{\partial \nu_2} & \cdots & \frac{\partial \mathbf{h}}{\partial \nu_Z} \end{bmatrix} \\ &= \begin{bmatrix} \left([\mathbf{A}_r]_{:,1} \otimes [\mathbf{A}_t]_{:,1} \otimes \frac{\partial [\mathbf{A}_d]_{:,1}}{\partial \nu_1} \otimes [\mathbf{A}_f]_{:,1} \right) \beta_1 & \cdots \\ ([\mathbf{A}_r]_{:,Z} \otimes [\mathbf{A}_t]_{:,Z}) \beta_Z \otimes \frac{\partial [\mathbf{A}_d]_{:,Z}}{\partial \nu_Z} \otimes [\mathbf{A}_f]_{:,Z} \end{bmatrix} \\ &= (\mathbf{A}_r \diamond \mathbf{A}_t \diamond \mathbf{D}_d \diamond \mathbf{A}_f) \mathbf{X}\end{aligned}\quad (102)$$

where \mathbf{D}_d is defined similar to (99).

G. Derivative With Respect to η

Following a procedure similar to those presented above, the derivative of \mathbf{h} with respect to η can be shown to be

$$\frac{\partial \mathbf{h}}{\partial \eta} = (\mathbf{A}_r \diamond \mathbf{A}_t \diamond \mathbf{A}_d \diamond \mathbf{D}_f) \mathbf{X}\quad (103)$$

APPENDIX B

EVALUATION OF FIM AND ERROR BOUND

Once the derivatives of the channel observation \mathbf{h} and the covariance matrix have been obtained, the expression for the FIM and the prediction error bound are obtained by substituting the derivatives in Appendix A. Using (72) and (78), the matrix \mathbf{J} in (80) is obtained as

$$\mathbf{J} = \frac{\partial \mathbf{h}^H}{\partial \Theta} \frac{\partial \mathbf{h}}{\partial \Theta}\quad (104)$$

where

$$\begin{aligned}\frac{\partial \mathbf{h}}{\partial \Theta} &= \begin{bmatrix} \frac{\partial \mathbf{h}}{\partial \Re(\beta)} & \frac{\partial \mathbf{h}}{\partial \Im(\beta)} & \frac{\partial \mathbf{h}}{\partial \mu^r} & \frac{\partial \mathbf{h}}{\partial \mu^t} & \frac{\partial \mathbf{h}}{\partial \nu} & \frac{\partial \mathbf{h}}{\partial \eta} \end{bmatrix} \\ &= [\mathbf{A} \ j \mathbf{A} \ (\mathbf{D}_r \diamond \mathbf{A}_t \diamond \mathbf{A}_d \diamond \mathbf{A}_f) \mathbf{X} \ (\mathbf{A}_r \diamond \mathbf{D}_t \diamond \mathbf{A}_d \diamond \mathbf{A}_f) \mathbf{X} \\ &\quad (\mathbf{A}_r \diamond \mathbf{A}_t \diamond \mathbf{D}_d \diamond \mathbf{A}_f) \mathbf{X} \ (\mathbf{A}_r \diamond \mathbf{A}_t \diamond \mathbf{A}_d \diamond \mathbf{D}_f) \mathbf{X}]\end{aligned}\quad (105)$$

With \mathbf{G}_1 – \mathbf{G}_5 as given in (81)–(85), (105) can be simplified to

$$\frac{\partial \mathbf{h}}{\partial \Theta} = \mathbf{G}_1 \diamond \mathbf{G}_2 \diamond \mathbf{G}_3 \diamond \mathbf{G}_4 \diamond \mathbf{G}_5\quad (106)$$

and (104) becomes

$$\mathbf{J} = (\mathbf{G}_1 \diamond \mathbf{G}_2 \diamond \mathbf{G}_3 \diamond \mathbf{G}_4 \diamond \mathbf{G}_5)^H (\mathbf{G}_1 \diamond \mathbf{G}_2 \diamond \mathbf{G}_3 \diamond \mathbf{G}_4 \diamond \mathbf{G}_5)\quad (107)$$

Using the properties of the Khatri-Rao and Hardamard products, (107) reduces to the form given in (80).

REFERENCES

- [1] G. Li and G. Stüber, *Orthogonal Frequency Division Multiplexing for Wireless Communications*, ser. Signals and Communication Technology. Springer Science+Business Media, 2006.
- [2] E. Dahlman, S. Parkvall, J. Skold, and P. Beming, *3G Evolution, Second Edition: HSPA and LTE for Mobile Broadband*, 2nd ed. Academic Press, 2008.
- [3] *Part 16: Air Interface for Broadband Wireless Access Systems*, ser. IEEE Standard for local and metropolitan area networks. IEEE, May 2009.
- [4] D. G. Edt, *Mobile WiMAX Part I: A Technical Overview and Performance Evaluation*, WiMAX Forum, 2006.
- [5] P. Xia, S. Member, S. Zhou, and G. B. Giannakis, "Adaptive MIMO-OFDM Based on Partial Channel State Information," *IEEE Trans. Sig. Proc.*, vol. 52, pp. 202–213, 2004.
- [6] M. Kountouris, T. Sälzer, and D. Gesbert, "Scheduling for multiuser MIMO downlink channels with ranking-based feedback," *EURASIP J. Adv. Signal Process.*, vol. 2008, pp. 131:1–131:14, Jan 2008.
- [7] S. B. Lande, J. B. Helonde, R. Pande, and S. S. Pathak, "Adaptive Subcarrier and Bit Allocation for Downlink OFDMA System with Proportional Fairness," *CoRR*, vol. abs/1111.2160, 2011.
- [8] A. Duel-Hallen, S. Hu, and H. Hallen, "Long Range Prediction of Fading Signals: Enabling Adaptive Transmission for Mobile Radio Channels," *IEEE Sig. Proc. Magazine*, vol. 17, pp. 62–75, 2000.
- [9] D. Rhee, H. Hwang, Y. Sang, and K. Kim, "Multiuser adaptive transmission technique for time-varying frequency-selective fading channels," *Signal Processing*, vol. 88, no. 8, pp. 2095–2107, 2008.
- [10] T. Ekman, "Prediction of Mobile Radio Channels — Modeling and Design," Ph.D. dissertation, Uppsala University, 2002.
- [11] G. E. Oien, H. Holm, and K. J. Hole, "Impact of channel prediction on adaptive coded modulation performance in Rayleigh fading," *IEEE Trans. on Vehicular Technology*, vol. 53, pp. 758–769, 2004.
- [12] J. Andersen, J. Jensen, S. Jensen, and F. Frederisen, "Prediction of future fading based on past measurements," in *IEEE Vehicular Technology Conference*, vol. 1, 1999, pp. 151–155.
- [13] I. C. Wong and B. L. Evans, "Sinusoidal Modeling and Adaptive Channel Prediction in Mobile OFDM Systems," *IEEE Trans. on Sig. Proc.*, vol. 56, no. 4, pp. 1601–1615, 2008.
- [14] R. Vaughan, P. Teal, and R. Raich, "Short-term mobile channel prediction using discrete scatterer propagation model and subspace signal processing algorithms," in *IEEE Vehicular Technology Conference*, vol. 2, 2000, pp. 751–758.
- [15] J. Liu and X. Liu, "Time-varying channel identification and prediction in OFDM systems using 2-D frequency estimation," in *Proceedings of the 2006 IEEE Conference on Military Communications*, ser. MILCOM'06. Piscataway, NJ, USA: IEEE Press, 2006, pp. 2777–2783.
- [16] B. Yang, K. B. Letaief, R. S. Cheng, and Z. Cao, "Channel estimation for OFDM transmission in multipath fading channels based on parametric channel modeling," *IEEE Trans. on Communications*, vol. 49, no. 3, pp. 467–479, aug 2002.
- [17] P. Teal and R. Vaughan, "Simulation and performance bounds for real-time prediction of the mobile multipath channel," in *IEEE Workshop on Statistical Signal Processing Proceedings*, 2001, pp. 548–551.
- [18] A. Arredondo, K. R. Dandekar, and G. Xu, "Vector channel modeling and prediction for the improvement of downlink received power," *IEEE Trans. on Comm.*, vol. 50, no. 7, pp. 1121–1129, 2002.
- [19] T. Svantesson and A. Swindlehurst, "A performance bound for prediction of MIMO channels," *IEEE Trans. on Sig. Proc.*, vol. 54, no. 2, pp. 520–529, Oct 2006.
- [20] M. Larsen, L. Swindlehurst, and T. Svantesson, "A Performance Bound for MIMO-OFDM Channel Estimation and Prediction," in *Proc. Fifth IEEE Sensor Array and Multichannel Signal Processing Workshop*, 2008, pp. 141–145.
- [21] K. Okino, T. Nakayama, S. Joko, Y. Kusano, and S. Kimura, "Direction based beamspace MIMO channel prediction with ray cancelling," in *Proc. IEEE PIMRC*, 2008, pp. 1–5.
- [22] J. Chang, I.-T. Lu, and Y. Li, "Adaptive Codebook Based Channel Prediction and Interpolation for Multiuser MIMO-OFDM Systems," in *ICC*, 2011, pp. 1–5.
- [23] T. Inoue and R. W. Heath, Jr., "Grassmannian Predictive Coding for delayed limited feedback MIMO systems," in *Proceedings of the 47th annual Allerton conference on Communication, control, and computing*, ser. Allerton'09. Piscataway, NJ, USA: IEEE Press, 2009, pp. 783–788.
- [24] B. Godana and T. Ekman, "Linear prediction of time-varying MIMO systems using Givens rotations," in *IEEE Workshop on Signal Processing Advances in Wireless Communications*, 2011, pp. 371–375.
- [25] J. Vanderpypen and L. Schumacher, "MIMO Channel Prediction using ESPRIT based Techniques," in *Proc. IEEE PIMRC*.
- [26] M. D. Larsen, A. L. Swindlehurst, and T. Svantesson, "Performance bounds for MIMO-OFDM channel estimation," *IEEE Trans. on Sig. Proc.*, vol. 57, no. 5, pp. 1901–1916, May 2009.
- [27] R. Roy and T. Kailath, "Estimation of signal parameters via rotational invariance techniques," *IEEE Trans on Acoustics, Speech, Signal Processing*, vol. 37, pp. 984–995, Jul 1989.
- [28] "IST-WINNER II Deliverable 1.1.2 v.1.2, WINNER II channel models," IST-WINNER2, Tech. Rep., 2007.
- [29] M. Wax and T. Kailath, "Detection of signals by information theoretic criteria," *IEEE Trans. on Acoustics, Speech and Signal Processing*, vol. 33, no. 2, pp. 387–392, 1985.
- [30] S. M. Kay, *Modern Spectral Estimation: Theory and Application*. Prentice Hall.

- [31] L. Huang, T. Long, E. Mao, H. C. So, and S. Member, "MMSE-Based MDL Method for Accurate Source Number Estimation," *IEEE Signal Processing Letters*, vol. 16, no. 9, pp. 798–801, 2009.
- [32] N. Kikuma, H. Kikuchi, and N. Inagaki, "Pairing of Estimates Using Mean Eigenvalue Decomposition in Multi-Dimensional Unitary ESPRIT," *IEEE Trans.*, vol. J82-B, no. 11, pp. 2202–2207, Nov 1999.
- [33] S. M. Kay, *Fundamentals of statistical signal processing: estimation theory*. Upper Saddle River, NJ, USA: Prentice-Hall, Inc., 1993.
- [34] P. Kysti, J. Meinilä, L. Hentilä, X. Zhao, T. Jms, C. Schneider, M. Narandzi, M. Milojević, A. Hong, J. Ylitalo, V.-M. Holappa, M. Alatossava, R. Bultitude, Y. de Jong, and T. Rautiainen, "WINNER II Channel Models," Tech. Rep., Sep 2007.